



# Treball Final de Grau

**Liquid phase segregation in lipid bilayers: an experimental and computational approach**

**Segregació de fases líquides en bicapes lipídiques: una aproximació experimental i computacional**

Anna Cardenal Rodriguez

*June 2019*



UNIVERSITAT DE  
BARCELONA

**B:KC** Barcelona  
Knowledge  
Campus  
Campus d'Excel·lència Internacional



Aquesta obra esta subjecta a la llicència de:  
Reconeixement–NoComercial–SenseObraDerivada



<http://creativecommons.org/licenses/by-nc-nd/3.0/es/>



*"There is a way out of every box, a solution to every puzzle; it's just a matter of finding it."*

Cpt. Jean-Luc Picard, ST: TNG.

First and foremost, I'd like to dedicate this report to my parents, for supporting me always, and even more so throughout these last years. I'd also like to thank Dr. Ramon Reigada for his unending help and counsel, and for guiding me through the whole process. Finally, I'd also like to thank my lab mates from Laboratory 4017 for their help and company, and my class partners for the last four years we've shared together. All of you have truly made an impact in my life, and I could not be more grateful.



**REPORT**





# CONTENTS

<b>1. SUMMARY</b>	3
<b>2. RESUM</b>	5
<b>3. INTRODUCTION</b>	7
3.1. Cell membrane and lipid rafts	7
3.2. Leaflet segregation and interleaflet correlation	9
<b>4. OBJECTIVES</b>	11
<b>5. METHODOLOGIES</b>	11
5.1. Experimental methods	12
5.1.1. Solutions and material procedures	12
5.1.2. Electroformation	12
5.1.3. Vesicle observation and characterization	15
5.2. Computational methods	18
5.2.1. Coarse-graining approach	18
5.2.1. Simulated molecules	19
5.2.1. Simulation protocols	20
<b>6. RESULTS</b>	21
6.1. Experimental results	21
6.2. Computational results	24
<b>7. CONCLUSIONS</b>	30
<b>8. REFERENCES AND NOTES</b>	35
<b>9. ACRONYMS</b>	37
<b>APPENDICES</b>	39
Appendix 1: Mean squared displacement graphics	41



# 1. SUMMARY

The study of the eukaryotic cell membrane lipid bilayer and its functionality is of paramount importance to determine processes involved in signal transduction, transmembrane protein activity, etc... Up until the 1980s, the fluid mosaic was commonly used to describe cell membranes, but from there on the lipid raft model was proposed. According to the theory, the lipid composition of bilayers is not homogenous, but rather microdomains rich in saturated lipids and cholesterol which are more rigid and less permeable, and “float” in a liquid-disordered phase, rich in unsaturated lipids. The aim of this report is to study the structure of lipid bilayers with liquid phase segregation with both experimental and computational approaches. The bilayers mimic the complex, lipid-raft based structure of in vivo membranes via the formation of liquid phases in ternary vesicles.

Electroformation of lipid vesicles was carried out with three different compositions (DOPC, DPPC/CHOL, DOPC/DPPC/CHOL), whose amount and diameter were quantified using optical microscopy. DOPC vesicles are the smallest but most abundant, whereas DPPC/CHOL vesicles are the least abundant but the biggest. Ternary vesicle lie between the two extreme cases. Using fluorescence optical microscopy, liquid-ordered and disordered phases are observed, as well as occasionally pear-shaped vesicles due to differences in surface tension

Coarse-grained molecular dynamics simulations in explicitly hydrated nanometric boxes with periodic boundaries were carried out, at three different temperatures. DOPC was used as an unsaturated lipid, as well as two different saturated lipids with different aliphatic chain length, DLPC and DSPC and cholesterol. Liquid phase segregation was observed, as well as anticorrelation phenomena between bilayer leaflets in DSPC-rich bilayers. Furthermore, the lateral diffusion coefficient for each chemical species was calculated from the mean squared displacement of the last part of each simulation and compared and contrasted with experimental and other computational results to confirm they are realistic. DOPC is more mobile than their saturated counterparts, which fits the lipid raft model previously discussed.

**Keywords:** coarse grained, electroformation, fluorescence optical microscopy, lateral diffusion coefficients, lipid bilayer, liquid-disordered phase, liquid-ordered phase, molecular dynamics, vesicles

## 2. RESUM

L'estudi de la bicapa lipídica de la membrana cel·lular eucariòtica és de rellevant importància per determinar processos involucrats en la transducció de senyals, l'activitat de proteïnes transmembrana, etc... Fins els anys 80, el model del mosaic fluid era usat comunament per descriure les membranes, però es va proposar el model dels *lipid rafts*. Segons aquest model, la composició lipídica de les bicapes no es homogènia, si no que es formen microdominis rics en lípids saturats i colesterol, que son més rígids i impermeables, que "floten" en una fase líquida desordenada, rica en lípids insaturats. L'objectiu d'aquest report és estudiar la estructura de bicapes lipídiques amb separació de fases líquides amb una aproximació tant experimental com computacional. Les bicapes a estudiar imiten la estructura complexa i basada en *lipid raft* de les estructures in vivo de les membranes cel·lulars, per camí de la formació de fases líquides en vesícules ternàries.

La electroformació de vesícules lipídiques es du a terme fent servir tres composicions (DOPC, DPPC/CHOL, DOPC/DPPC/CHOL), la quantitat i diàmetre de les quals es quantifica fent servir microscòpia òptica. Les vesícules de DOPC són les més petites i abundants, mentre que les de DPPC/CHOL són les menys abundants però més grans. Les vesícules ternàries constitueixen un cas intermedi entre aquests extrems. Usant microscòpia òptica de fluorescència, les fases ordenada i desordenada són observables, així com vesícules amb forma de pera a causa de diferències de tensió superficial.

Les simulacions de dinàmica molecular *coarse-grained* es duen a terme en caixes nanomètriques explícitament hidratades, a tres temperatures diferents. DOPC es el lípid insaturat escollit, així com dos lípids saturats amb diferent llargada de cadena alifàtica, DLPC i DSPC. S'observa segregació de fases líquides, així com fenòmens d'anticorrelació entre capes de la vesícula en bicapes riques en DSPC. A més a més, els coeficients de difusió lateral per cada espècie química es calculen a partir del desplaçament quadràtic mitjà de l'última part de cada simulació, i es comparen i contrasten amb dades experimentals així com computacionals per confirmar que són valor realistes. DOPC és més mòbil que els equivalents saturats, la qual cosa s'ajusta al model de *lipid rafts* mencionat anteriorment.

**Paraules clau:** coarse grained, electroformació, microscòpia òptica de fluorescència, coeficients de difusió lateral, bicapes lipídiques, fase líquida desordenada, fase líquida ordenada, dinàmica molecular, vesícules

### 3. INTRODUCTION

#### 3.1. CELL MEMBRANE AND LIPID RAFTS

Eukaryotic cell membranes, such as the ones humans possess, are mainly formed by a liquid lipidic bilayer which is selectively permeable to apolar substances. The main components of the bilayer are phospholipids, which are formed by a glycerol molecule bonded to two fatty acids, as well as a phosphate group. Phospholipids are amphiphilic molecules, which constitute a glycerol molecule bonded to two fatty acids and a phosphate group via ester bonds, with a polar head and a longer apolar tail. The amphiphilic nature deeply affects the structure of the bilayer: two layers of phospholipids with their apolar tails facing inwards, and their respective polar heads facing the cytoplasm on one side and the extracellular matrix on the other (Figure 1).

Other components of the membrane are sphingolipids, glycolipids, cholesterol, proteins... It constitutes the barrier between each cell and the rest of the body, and thus it is deeply involved in regulating chemical pathways and reactions, as well as anchoring and communicating the cell with its environment.

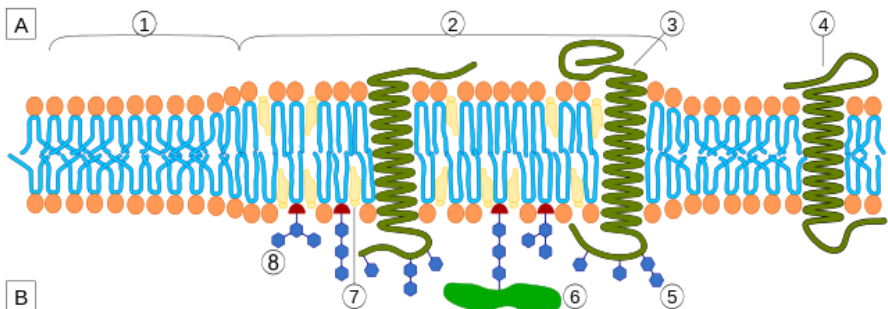


Figure 1. Transversal scheme of eukaryotic cell membrane. 1:  $L_d$  phase, 2:  $L_o$  phase, or lipid raft.

7: cholesterol

(Author: Artur Jan Fijałkowski, 24/05/2019 via Wikimedia Commons, Creative Commons Attribution)

The composition and structure of cell membranes, however, is not homogenous. Up until the 1980s, it was thought that proteins and lipids were distributed randomly, following the fluid mosaic model. The existence of microdomains enriched with glycosphingolipids and sterols, and with tighter packing and ordering, called lipid rafts, was first proposed [1]. As their name indicates, and because of their tighter packing due to the action of the cholesterol over the saturated aliphatic chains, denser microdomains that still retained liquid properties are formed, and thus yielding coexisting liquid phases in a lamellar regime.

These phases are commonly known as liquid-ordered and liquid-disordered (shortened to  $L_o$  and  $L_d$ , respectively). Furthermore, said lipid rafts can diffuse around the membrane, with fluidity and might regulate not only the trafficking across the membrane, but also its activity [2], in processes such as signal transduction [3]. For example, said regulation processes might be involved in neurotransmission, and due to malfunction be also related to several nervous system diseases [4].

The first inconvenient of this hypothesis, however, was that rafts are in the nanoscale, and thus invisible to conventional optical microscopy, which led to skepticism about their existence [5]. However, some alternatives for membrane lipid imaging have arisen, such as fluorescence microscopy [6] or neutron scattering and diffraction in isotopically labeled membranes [7], which have provided evidence for the existence of lipid rafts. Molecular dynamics computer simulations have also been used to reproduce the spontaneous formation of two-phase lipidic vesicles and their boundary dynamics at an atomic level [8], as well as protein distribution across the membrane microdomains [9].

Due to the constraints of both time and resources, and because biological systems possess a complexity that is hard to replicate and control in laboratory conditions, simplified lipid vesicles, also known as liposomes, will be used to carry out my experimentation. The lipid family chosen is that of the phosphatidylcholines (PC), which as their name indicates, have a choline group attached to the phosphate group. Specifically, DOPC will be used as an unsaturated lipid, and DPPC and cholesterol to mimic lipid rafts, (Figure 2) and thus obtain  $L_o/L_d$  systems at a bigger scale [10], using biologically coherent concentrations. The vesicles will be prepared via electroformation in an ITO electroforming cell with oscillating alternate current [11].



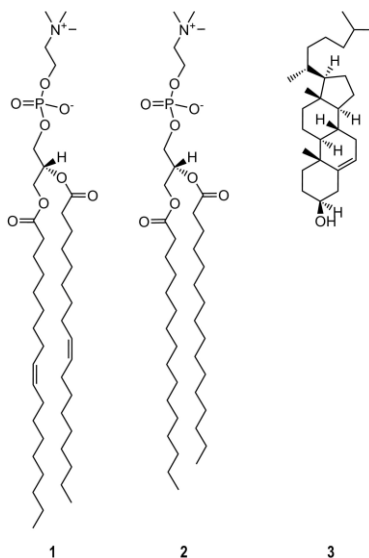


Figure 2: Components of electroformed lipid vesicles. 1: DOPC, 2: DPPC, 3: cholesterol

### 3.2. LATERAL SEGREGATION AND INTERLEAFLET CORRELATION

The experimentation can be complemented with MD simulations using GROMACS [12]. Molecular dynamics allows us to simulate numerically biological systems at very small space and time scales. However, the time scale to resolve the calculations at an atomic scale greatly exceeds that of the time allotted. For that reason, a specialized force field MARTINI has been created [13], which provides a CG (coarse grained) model that greatly simplifies the calculation of biological processes taking place at the microsecond scale.

The main objective of carrying out MD simulations is to “observe” phenomena that is not visible at micrometric scale or using conventional optical microscopy, in order to complement the experimental findings. Specifically, I would like to observe the same liquid lipidic domain lateral segregation from a randomly generated lipidic bilayer with biologically coherent composition, which would form  $L_o/L_d$  domains at the nanoscale, upon which the lipid rafts theory is based on.

The driving force of this segregation is the lateral interaction between lipids and non-complete miscibility between lipids. The most remarkable lateral interaction is cholesterol causing a condensation effect amongst saturated lipids [14, 15], which results in an increase of rigidity and a decrease of permeability, whilst maintaining bilayer fluidity. Cholesterol interacts

more favorably with the straight, long aliphatic chains of saturated lipids, and allows for tighter packing. That by itself doesn't cause segregation, but when combined with unsaturated lipids that do not show the same behavior due to tilted chains and less dense packing, segregation occurs. There have been studies wherein lipid mixtures containing saturated lipids, unsaturated lipids and cholesterol were studied at different compositions with membrane models, ternary diagrams where elaborated and coexistence of two liquid phases was found [10, 16].

I also expect to capture correlation and anticorrelation phenomena between the same kind of liquid phase on either leaflet of the simulated membrane, depending on the chain length difference between lipids on the  $L_o$  phase and the  $L_d$  phase. The two possible observable cases are correlation between  $L_o$  domains on either leaflet of the bilayer, or anticorrelation between  $L_o$  domains on either leaflet.

The biological relevance of these synchronization/desynchronization phenomena between leaflets of lipid bilayers radiates from the effect it has beyond the mere structure in the case of cell membranes, and in the realm of functionality of the actual membrane. Anticorrelation of domains causes changes in the curvature of the membrane. Ionic channels such as alamethicin [17] and transmembrane proteins such as rhodopsin [18] are sensitive to spontaneous curvature properties, which are dependent on lipid composition on their surroundings, and modulate their activity via conformation change. In the case of rhodopsin, this conformation change acts as a trigger of the visual excitation process. Similar behavior has been studied in phospholipases [19].

Correlation between domains is also being studied as a regulator or inhibitor of signal transduction through the membrane [20]. Furthermore, membrane proteins may not have the same affinity for each liquid phase depending on their peptide sequence and their ternary structure. Lipid shells that adhere to the surface of membrane proteins [21] or signals have been proposed, that also affect the affinity of said molecules to either liquid phase.

To sum up, studying the behavior of lipid segregation and structure of liquid phase domains in lipid bilayers might help understanding the whole of cell membrane functionality to a new degree, beyond the proteins it contains and its basic separation function. The use of molecular dynamics and computational means also eases the process of observing complex biological systems and helps us predict and explore future developments.

## 4. OBJECTIVES

The scope of this study is to characterize electroformed lipid vesicles with varying composition and observe phase segregation *in vitro*, while complementing the study of lipid rafts with MD simulations at different lipid compositions and temperatures of randomly generated lipid membranes. The following are specific objectives

To successfully produce lipid vesicles with three different compositions (DOPC, DPPC/CHOL and DOPC/DPPC/CHOL) using electroformation.

To characterize the number and size of the vesicles produced depending on their composition.

To observe the liquid-ordered and disordered phases in ternary vesicles, which mimic the lipid raft structure of *in vivo* membranes, using fluorescence microscopy.

To run MD dynamics simulations using a CG model and randomly generated bilayers to observe phase segregation overtime.

To run MD dynamics with saturated lipids with different chain lengths and temperatures, and observe possible phase morphology changes.

To extract qualitatively conclusions about the structure and stability of the vesicles prepared from both the experimental and MD results.

## 5. METHODOLOGIES

In this next section of the report, I will address the experimental procedures carried out in the lab and their specifics. These will include both the preparation of the lipid solutions, the vesicles, and the observation protocols, as well as the steps necessary to carry out the MD simulations.

## 5.1 EXPERIMENTAL

### 5.1.1 Solutions and material procedures

Firstly, the solutions with the different mixtures of lipids must be prepared in their correspondent biologically cohesive proportions. Three different kinds of solutions will be prepared, which contain different types of lipids in variable concentrations. In all solutions, however, the total concentration of lipids dissolved must not exceed 0.5 mg/mL, to ensure complete solvating.

The first solution contains only DOPC (unsaturated) at 0.5 mg/mL. The second one contains DPPC (saturated) and cholesterol at 73:27 molar, because cholesterol is usually at around 30% molar composition in human cell membranes. Finally, the third and last solution that is used will be the one that resembles actual human cell membranes the most. It contains DOPC and DPPC at around 1:1 molar relation, and around 30% molar of cholesterol as well, so I can observe both the  $L_d$  and  $L_o$  phases present at once. The final molar relation between DOPC/DPPC/Chol comes to 0.342:0.340:0.320. Furthermore, to differentiate the ordered and disordered phases I use a fluorescent probe that tends to segregate completely to one of these phases when the vesicles form. The probe selected is 14:0 NBD-DMPE, which tends to migrate to the  $L_o$  phase, at around 2% w/w concentration.

The lipids are weighed while they are still frozen, to ease the procedure, in an analytical balance with 5 decimals and dissolved in analytical grade chloroform. The mixture is stored in a frosted neck glass vial, sealed with thread tape, inside a refrigerator. ITOs, like the rest of the instrumental in the experimental procedures, must be managed and cleaned with and only with ultrapure water, such as milliQ water, and micro90, as not to pollute the samples as well as not to interfere with the efficiency of the electroforming process. Because the vesicles will be in a solution, it is easier to build a platform to pour and contain said solution and observe it through the microscope. For this purpose, DOWSIL 184 Silicone Elastomer Kit is used to prepare silicone wells to contain the solution, of 5 x 5 mm.

### 5.1.2. Electroformation

The main objective of this step is to make the lipids interact with each other laterally, so they start to arrange themselves to form bilayers. I do so by putting them in an aqueous but poor in electrolytes medium between two conducting glasses connected to an oscillating, alternate

current generator. By using a saccharose solution prepared with ultrapure water, I ensure the electrolyte amount is minimal, and thus there is no current passing through the solution when connected to the generator. Instead, only the potential oscillates, and so does the dipole at the polar head of the PCs, due to the charges present (positive in the choline, negative in the phosphate) in order to align itself with the electrical field. When in complete contact with water, the aliphatic chain that interacted with the glass previously, is repulsed by the polar solvent, and the lipids start to flip flop and arrange themselves in a more stable manner. Thus, the vesicles are formed. This process is commonly known as electroformation [11]:

1. Two clean, cut ITO glass slides are rinsed with water, and then dried with air. The conducting side of the glass slide is found using a multimeter, with the auditory signal mode, by pressing both electrodes on each side. The conducting side can be “seen” at naked eye as well by finding the side of the glass that possess a slightly darker coloration.
2. Two copper electrodes are then stuck with the metal part up, making sure that when they are put them together, each one is touching the other glass slide. Double sided adhesive tape is used.
3. Using wax, I form a noodle in a J shape to close off the area of one of the glasses that will contain the solution with the lipids. The upper part of the J must be left outside.
4. Two drops of 5  $\mu\text{L}$  of lipid solution are dropped at the center of the area closed off by the wax. The drops are let slowly, without separating the tip of the pipette from the drop. The drops are next to each other, not overlapping, and I wait until the chloroform dries completely.
5. The vial is once again covered with a frosted glass cap and sealed it with thread seal tape. I make sure the lower part of the cap starts to dry once the tape is in place, which indicates that the sealing is done. Store it again in the fridge until next use.
6. The ITOs are then put together, one in front of the other, and held in place with a clamp in each side. Using a micropipette, around 400-500  $\mu\text{L}$  of a 200 mM aqueous saccharose solution are put inside the area closed of by the wax and the glasses, until a meniscus forms on top.
7. Carefully, and without letting any air bubbles come in, the upper part of the wax J shape is brought down to cover the meniscus and seal off the contents of the electroforming cell. If bubbles get in, and because of the amphiphilic character of the

lipids, they will eventually migrate to the interphase between the air and the water, and therefore the amount of vesicles formed will diminish drastically.

8. Once the cell is sealed, the current generator is set to 1 V and 2 Hz, and switched on. The crocodile clamps are connected, one to each of the two cables connected to the electrodes (Figure 3). The cell is left connected overnight, the average length of time is usually around 16 hours.
9. After this period has passed, and using a micropipette with the tip cut, in order to avoid the new vesicles from passing through a tight space and be subjected to high pressure that might break them, the contents of the cell are transferred to a 1 mL Eppendorf tub, labeled, sealed with thread seal tape, and stored in fridge until further use.
10. The components of the cell are disassembled and dried. The wax is discarded and the electrodes are stored in a box, as they can be reused after thorough cleaning with basic solutions.

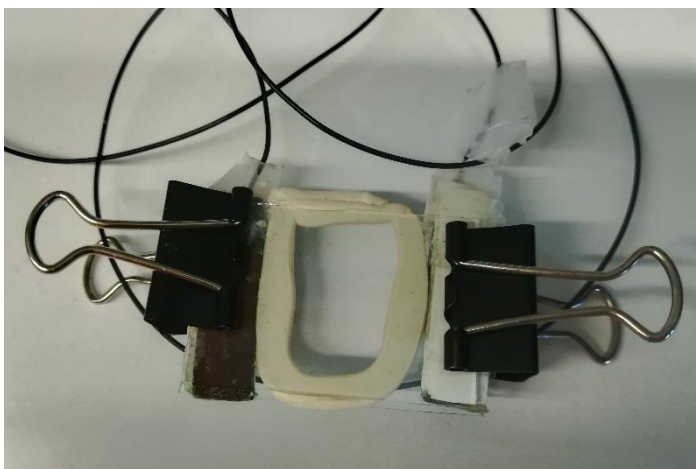


Figure 3: Connected electroformation cell

Now that vesicles have formed, I may proceed to characterize them using the microscope by measuring and counting them. The vesicles must not be shaken violently to avoid bursting. It is not recommended to preserve the vesicles for more than a week, because they might burst overtime. However, some of the samples have been shown to last upwards 2 weeks with minimal bursting, in the case of DPPC/Chol.

### 5.1.3 Vesicle observation and characterization

In order to observe the vesicles, I first must prepare a silicon well that is joined to a glass slide. A well is perforated all the way through using a punch extractor and a scalpel, conserving the circular and flat shape of the walls. The textured side of the well is put on top of a glass slide, with the channels in it horizontally. Using optical glue, I put some drops on the sides, and wait. Due to capillarity, the channels will fill from each side and meet halfway.

Once all the channels are filled, use a UV lamp at 70% intensity and irradiate for 10 seconds the glass slide until the glue solidifies. ALWAYS use UV-blocking glasses when operating the lamp. The contents of the Eppendorf that contains the vesicles must not be stirred. Using a cut 100  $\mu\text{L}$  micropipette tip, 60  $\mu\text{L}$  of a solution containing vesicles are pipetted, and dropped slowly in the center of the well. Make sure the tip and the drop maintain contact throughout the process. Otherwise, vesicles may burst or move along the walls of the well, instead of most remaining in the bulk.

Afterwards, 200mM glucose solution is added in the well with the same methodology, until a meniscus forms on top. This step is key for the vesicles to settle and be visible later. Cover the meniscus with a cover slip, making sure there are no bubbles underneath it. A good strategy is to put it vertically at one side and drop it slowly from left to right. Finally, the vesicles are left to settle at the bottom of the well for around 20-30 minutes, and the glass slide is then put under the microscope for observation.

Depending on the vesicle type or composition, the ideal observation methodology will vary. For DOPC, DPPC/Chol vesicles or ternary vesicles with no fluorescence, regular optical microscopy can be used. Here follow the specifications used in the experimentation:

- Microscope: Nikon Eclipse 6400 Pol
- Camera: Pixelink PL-4741
- Augmenting lense: x20
- Scale: 100  $\mu\text{m}$  – 300 px
- Lighting: minimal
- Filter: none or 6, depending on light conditions
- Capturing time: 10-40 ms

For ternary vesicles with fluorescence, an alternative source of light and filtering the correct wavelength is needed, so the specifications are slightly different:

- Microscope: Nikon Eclipse 6400 Pol
- Camera: Andor Ixon Ultra
- Augmenting lense: x20
- Scale: 100  $\mu\text{m}$  – 125 px
- Normal mode: 10 ms, no filter
- Fluorescence mode: 6000 ms, no light, LED on with red filter. I also use a carton hood to block most of the external light to enhance results. Increasing the exposure time will highlight the richest in fluorescent probe and diminish the background noise, and vice versa.

Phase contrast filters can also be used to enhance the contrast between vesicles and medium, if necessary, depending on external lighting conditions.

The final step of this section helps characterize the size distribution and amount of vesicles electroformed. This procedure can be done with a regular camera, for all vesicle types, granted there is good contrast between the vesicles and the environment. First, I obtain the perimeters of the vesicles formed:

1. Using the capturing software, take 10 pictures around the center of the well. Photos from the side of the well, due to interactions between the polymer and the vesicles, are not as representative of the sample.
2. Open ImageJ, and then drag and drop the picture you will analyze.
3. Because the plugin cannot measure the radius of the vesicles, go to Analysis > Set Measurements, and select both Area and Perimeter. Using commonplace formulas, the radius can be calculated approximately from both properties.
4. Next, both brightness and contrast will be changed to make the vesicles stand out more in the image. Go to Image > Adjust > Brightness/Contrast (shortcut Ctrl+Shift+C), and then select Auto and Apply in that order.
5. Following this, the bandpass filter is used to illuminate the image equally, and therefore facilitate the threshold selection step. Go to Process > FFT > Bandpass filter and select OK.
6. Duplicate the image, because once the threshold is applied it cannot be modified from the original image. Do so by pressing Ctrl+Shift+D.



7. Now, select the threshold mode to highlight the borders of the vesicles. Go to Image > Adjust > Threshold (shortcut: Ctrl+Shift+T) and select Auto. You can also modify it slightly towards the right in the bottom slider, in order to highlight more vesicles, but keep in mind it will also highlight more other parts of the image that might not be of interest. If necessary, choose Process > Binary > Dilate
8. The vesicles will be detected and measured using a plugin. Go to Plugins > Segmentation > DRAQ5. The measured vesicles will appear highlighted in yellow and numbered in the ROI manager pop-up. Delete all the selections that do not proceed or are not correct using the ROI side bar, and then press shift and select the first and last listing.
9. Click Measure, and another pop-up screen will show with the measurement. In order to measure manually all the non-detected vesicles, select the oval brush tool from the tool bar and hold Ctrl+Shift to draw a circle along the vesicle border.
10. Press Ctrl+M to add the measurement to the table. Click anywhere in the image before measuring the next vesicle. If not, the measurements will be cumulative instead of independent.
11. Once all the vesicles are measured, copy the information from the table on an Excel spreadsheet. To repeat the process, close all windows except the one containing the tool selection bar.

Then, I move on to analyze the data obtained. The median size, size distribution and number of vesicles resulting from each lipid mixture undergoing electroformation is accounted for using a histogram. The methodology is to be as consistent as possible when analyzing the pictures. Pictures analyzed only belong to the center of the well, due to irregular and misrepresentative distribution found along the edges of the well due to vesicles sticking, bursting and decreasing in size. 10 images are taken in a grid-like manner in the center of the well, making sure they have a similar number of vesicles in each one, regardless of their actual sizes. Then, the images are analyzed using the previously mentioned methodology. In this case, the perimeter is used to calculate the diameter of each vesicle in micrometers, presupposing that they are spherical in shape. Afterwards, the data will be exhibited in a histogram, and the average diameter of each type of vesicles is also calculated, to determine their relative size.

## 5.2 COMPUTATIONAL METHODS

### 5.2.1 Coarse-graining approach

The MARTINI force field allows us to carry out MD simulations of simplified biological systems [13] using a specifically parametrized bonding and non-bonding interactions, and discretized interaction sites. This allows me to simulate faster than atom-by-atom simulations, at the cost of some atomistic details. Bonding interactions are parametrized from all-atom simulations, whereas non-bonding interactions are calculated using a Lennard-Jones 12-6 potential energy function with discretized strengths depending on the affinity or repulsion between interaction centers [22].

The MARTINI force field is based on four-to-one mapping, in which four heavy atoms are represented as a single interaction center, and each four-atom group is characterized, parametrized and contrasted with experimental and thermodynamic data, and from there classified in one of four main types based on the interaction type: polar (P), apolar (C), non-polar (N), and charged (Q). Each type is then further characterized in several subtypes. For example, depending on their hydrogen bonding type (d, a, da or 0), or their degree of relative polarity if they are a P center (from 1 to 5, with 1 being the lowest). Lipids have four-to-one mapping [23], whereas cholesterol requires less discretization due to its cyclic nature, and thus uses three-to-one mapping [24].

For the MD of two-phase vesicles, I use the *insane* program [25] to generate a box system with the desired lipidic proportions already in a bilayer structure, with random distribution and hydration. From there, and with the file containing the topology of the molecules involved, the simulation is run using the GROMACS MD package [12]. In short, GROMACS first calculates the potential energy of all interaction centers using the parameters provided by MARTINI force field, distinguishing between intra (bond, angle, torsions...) and intermolecular (electrostatic, Van der Waals forces...) interactions. Then, it solves the derivative of the potential energy to obtain the forces, and then finally solves Newton's motion equations for the predetermined time step. This process is repeated with the previously obtained coordinates until all time steps are done. The final result of the simulation is a trajectory which contains the evolution of the system overtime. Longer systems and timescales, therefore, involve longer calculation times. The trajectory data can also be analyzed to obtain further information about the system, such as area per lipid, bilayer thickness, lateral diffusion rates, etc...

## 5.2.2 Simulated molecules

As previously mentioned, the *insane* program will be used to generate lipidic bilayers with known composition and random distribution. The molar concentrations will be similar to the ones used in experimental conditions, 1:1:0.3 for saturated, unsaturated and cholesterol respectively. In this batch of simulations, DUPC will be the unsaturated PC, while there will be two saturated PC types: DSPC and DLPC (Figure 4). DLPC has a shorter chain length than DSPC, and when applying CG modeling, that translates to two less interaction centers in four-to-one mapping. DUPC also has one more unsaturation than DOPC.

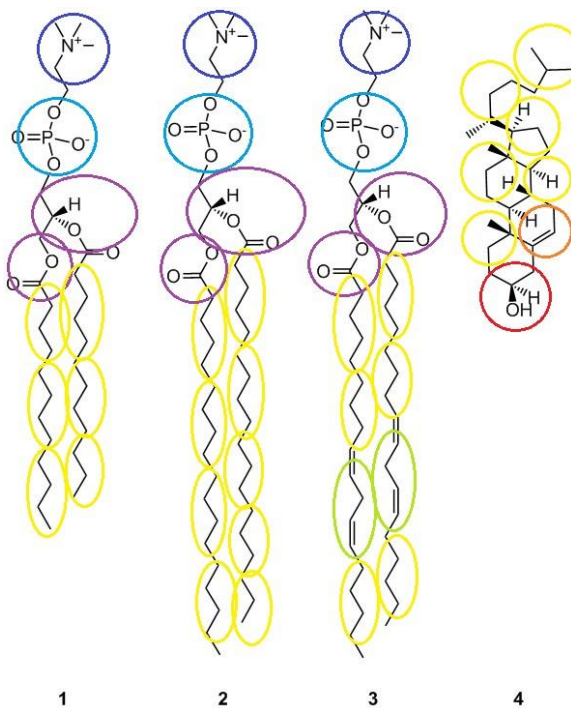


Figure 4: Simulated molecules: 1: DLPC, 2: DSPC, 3: DUPC, 4: cholesterol. Colored circles show MARTINI mapping

This is done to speed up the calculations and will come into play in the study of the liquid phases' morphology change. Water molecules are explicit and simulated as well, but their quantity in the box is regulated by the *insane* program depending of the hydration needed. In Figure 4, it can be seen that the aliphatic chains of the lipids have C1 interaction centers, with

represent the highest degree of apolarity, and the unsaturated centers have a C4 type interaction, which is less apolar. The choline group has a Q0 type center, which represents that it is charged but does not act as a donor or acceptor of hydrogen bonds. The phosphate group is Q type, but has a subtype, because it can accept hydrogen in a hydrogen bond. As was commented on before, cholesterol shows a higher discretion level for mapping.

### 5.2.3 Simulation protocols

*Insane* program provides the initial coordinates for the simulation, while the *top* file provides the topology of the molecules, as well as calling the *itp* files that contain both the force field parameters and charges. Energy minimization is first carried out using the steepest descent mode, before the MD simulation proper. Energy minimization detects unfavorable overlaps and interactions and corrects them to avoid crashes and longer simulation times. MD simulation can only be done after this minimization step. MD simulation is carried out in the IQTCUB computer cluster, due to its highly demanding CPU time and capabilities.

All simulations have the same time step of 0.01 fs. They also have the same cubic box size of 20 nm, with periodic boundary conditions. This last condition means that, when calculating energies, forces and movement, GROMACS will consider that in the adjoining directions of the simulation box in all axes, lie multiple versions of the same box, which makes it slightly similar to real conditions. Temperature and pressure coupling are also implemented. This option allows the box to, after a set period of time, check if there have been changes in these conditions and rectify them to previously set values by slightly modifying energies, speed, etc... in order to maintain conditions similar to that of an isothermal bath, in the case of temperature. Furthermore, pressure is established as a semisotropic constant in all simulations. This means that constant pressure of 1 bar is applied in the perpendicular axis to that of the bilayer plane, as well as in the xy parallel plane that contains the bilayer itself. However, these pressures are coupled independently from each other.  $\Delta t$ , or the recalculating step taken for the coupling, is of 1.5 ps for temperature and 3.0 ps for pressure. A cut-off distance of 1.2 ns for Van der Waals interactions is also implemented for all simulations.

Simulation length is the same for all systems: 1800 ns. However, it can be lengthened by 600 ns if a certain phase equilibrium is not reached, for example in the case of the bilayer containing DSPC at 295K. The trajectories and final state of the simulated systems are visualized and analyzed using VMD, which also allows us to visualize different chemical species

independently, represent energy surfaces, etc... The MSD for all chemical species is also computed, from a provided initial position of a trajectory. Specifically I use the last 600 ns of each simulation, once phase segregation is reached, and through these values the lateral diffusion coefficient of the phases is obtained.

## 6. RESULTS

In this following section of the work, I discuss the results of the experimentation. Firstly, I discuss the results of the first half of the work, which corresponds to experimental vesicle formation and characterization. Later, the results of the MD simulations, leaflet correlation phenomena and calculated lateral diffusion coefficients will be discussed.

### 6.1 Experimental results

Vesicles with three starkly different lipid compositions have been successfully prepared via electroformation in a reproducible manner, with vesicle amounts enough to allow systematic vesicle recount and measurement via image analysis. The three kinds of vesicles prepared are DOPC (unsaturated), DPPC/CHOL (saturated, 1:1 molar) and ternary vesicles containing DOPC/DPPC/CHOL (0.342:0.340:0.320 molar), mimicking the composition of eukaryotic cell membranes. Ternary vesicles also contain a fluorescent probe that has higher affinity with the  $L_o$  phase, and therefore will be shown with light coloration in fluorescence optical microscopy, with their  $L_d$  counterparts remaining dark.

After analyzing the images obtained using Image J, with the DRAQ5 plugin, and treating the data to obtain average diameters as well as size distribution histograms, the following results were obtained. First, almost vesicles are spherical in shape, due to the lowering of the surface area to volume ratio effect on the stability of the vesicles. Their size ranges between 5 to 70  $\mu\text{m}$ , depending on the composition, with 10-20  $\mu\text{m}$  being the most common size bracket (Figure 8). None of the vesicle types possess Gaussian size distribution. In Figure 5a, DOPC vesicles are observed, which are abundant but smaller in size, compared to their DPPC/CHOL counterparts (Figure 5b, Table 1). DPPC/CHOL have lower curvature due to the rigidity added by cholesterol, and thus can be bigger.

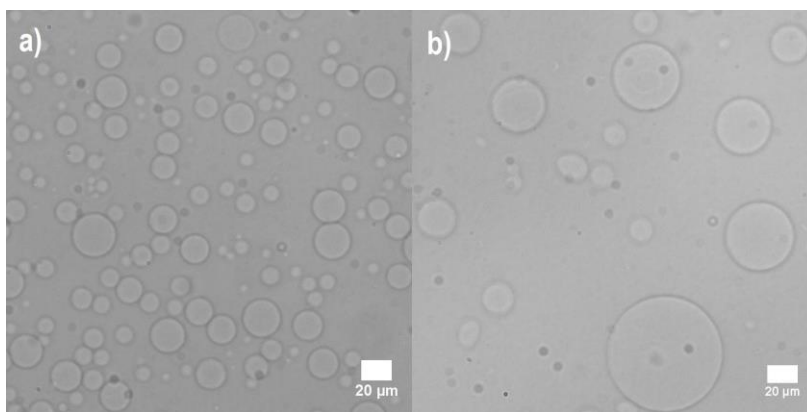


Figure 5: images of vesicles taken with Andor Ixon Ultra. A: DOPC, B: DPPC/CHOL

Ternary vesicles lie between these two extreme cases (Figure 6a), forming in lesser quantities but still slightly bigger than DOPC vesicles (Table 1). Cholesterol acts as the driving force behind phase segregation, as I previously mentioned in section 3.1, due to the condensation effect they cause in saturated lipids.

When they are put under fluorescence optical microscopy (Figure 6b), not all the vesicles present in Figure 6a show up, meaning they are entirely made up of  $L_d$  phase, and some vesicles are entirely lighted, which means they contain only  $L_o$  phase. However, vesicles with only half or part of the vesicle is  $L_o$  phase, which is lighted, and the rest is  $L_o$  are present in the sample. Therefore, phase segregation is actually observed experimentally.

Only ternary vesicles occasionally also show a pear-like shape (Figure 7), which is caused by the difference in surface tension between the liquid-ordered and disordered phases, showing

as two different curvatures in the same vesicle. The “bright” phase corresponds to the  $L_o$  phase, where the probe is located.  $L_o$  phase tends to display lower curvatures than the  $L_d$  phase, due to the rigidity provided by the presence of cholesterol and tighter packing.

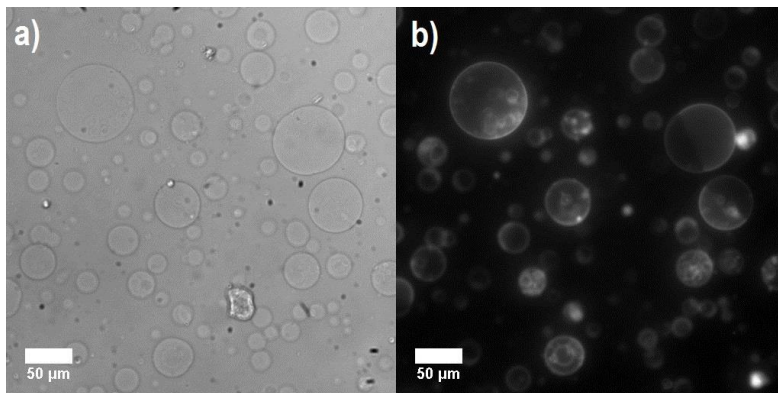


Figure 6: images of ternary vesicles taken with Andor Ixon Ultra. A: regular lighting, B: fluorescence.

Illuminated areas correspond to  $L_o$  phase

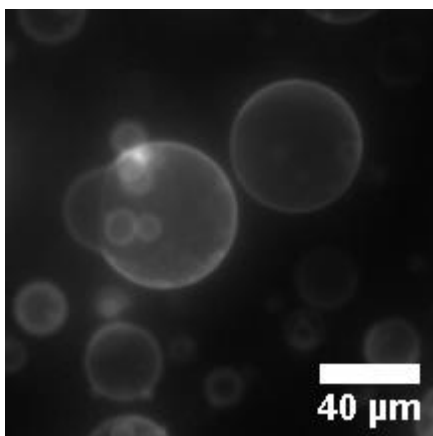


Figure 7: pear shaped ternary vesicle, taken with Andor Ixon Ultra

Entry	Vesicle type	Average diameter [ $\mu\text{m}$ ]	Average n. ves./image	Total vesicles
1	DOPC	14,67	218	1887
2	DPPC/CHOL	22	30	295
3	DOPC/DPPC/CHOL	15,77	51	465

Table 1: electroformed vesicles characterization data

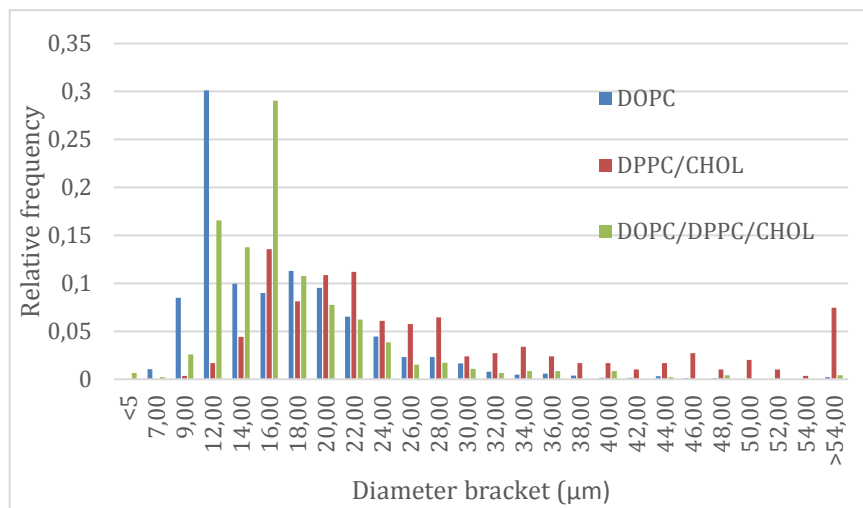


Figure 8: Vesicle diameter histogram with relative frequencies

## 6.2 Computational results

Simulations were run using the MARTINI CG force field and GROMACS of three cubic  $20 \times 20 \times 20$  nm boxes with periodic boundaries, with the same parameters and simulation length (1800 ns), but at three different fixed temperatures (285K, 290K, 295K) using an isothermal conditions. Half of the simulations have been done using DLPC (3 interaction sites in the aliphatic chain, see Figure 4.1), and the other half DSPC (which has a longer aliphatic chain, with 5 interaction sites, see Figure 4.2), as the saturated lipid, and cholesterol at biologically coherent concentration, giving us 1:1:0.3 molar concentration respectively. Trajectories and membrane images are obtained using VMD.



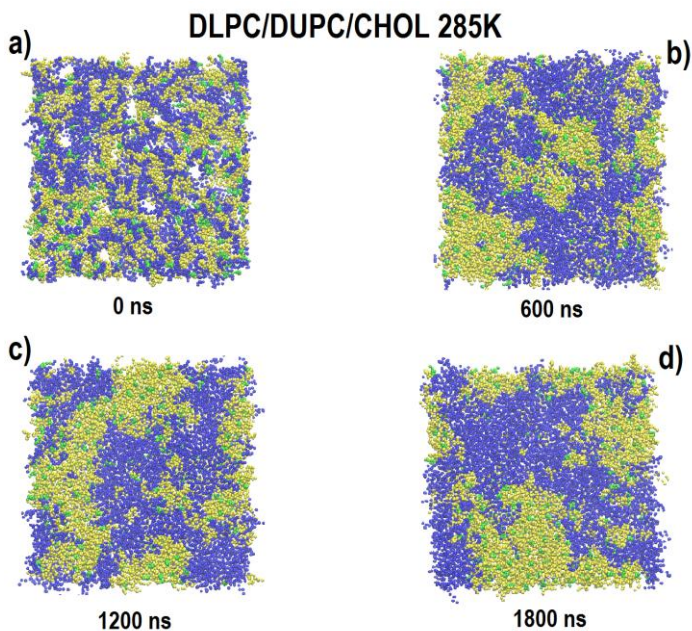


Figure 9: phase segregation sequence of DLPC containing bilayer at 285 K. Liquid phase formation can be observed. DLPC: yellow, main component of  $L_0$  phase

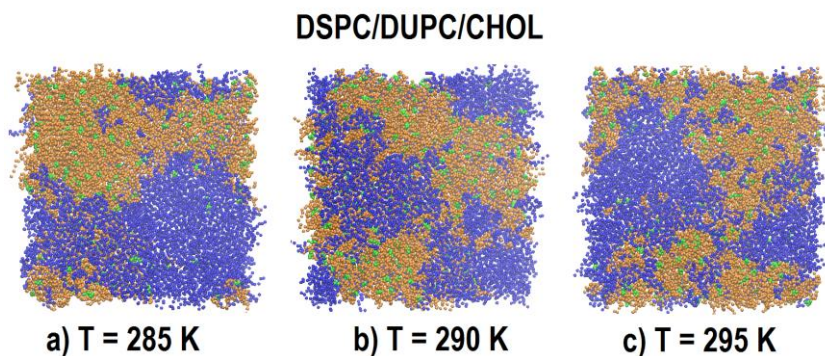


Figure 10: Domain fluctuation and shape depending on temperature for a same composition.

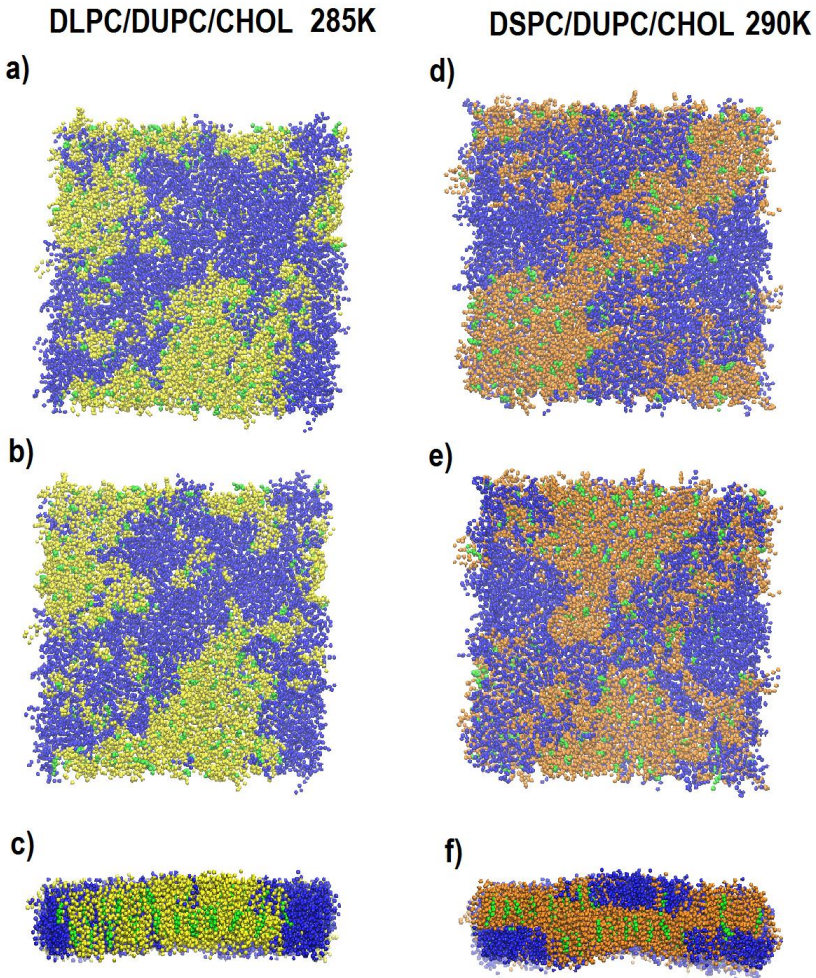


Figure 11: final states of simulations. a,b and d,e show either leaflet of the respective bilayer. c and f show the profiles. DLPC containing bilayer shows correlation, whereas the DSPC containing one shows anticorrelation.

In all cases, segregation between  $L_o$  and  $L_d$  is observed (an example of this process is Figure 9), and this segregation is generally slower at higher temperature. Furthermore, there are less fluctuating and rounded domains at lower temperatures, when the system has deeper quenching (Figure 10a). This is likely due to less thermally-related Brownian movement, and because the deeper the quenching, the more segregated and enriched with their respective

lipids the domains are and larger lineal tension. In Figure 11, the final conditions of simulations for both DLPC and DSPC containing bilayers can be seen. On the left, the domains on both sides (Fig. 11a,b) are more rounded and there is correlation between leaflets, which is more noticeable when looking at the side view (Fig. 11c).

Lateral phase separation is proposed to be entropy drive to keep the disordered unsaturated lipids away from the rafts, where they cannot be incorporated due to tight packing and cholesterol condensation effect [26]. Appearance of a stripped pattern in domains is attributed to the finite size box effect due to the use of periodic boundaries (Figure 11d,e) [8].

DLPC-enriched  $L_0$  domains generally show correlation of domains on both sides of the membrane, whereas DSPC-enriched  $L_0$  domains show anticorrelation (Figure 11f). Furthermore, anticorrelated domains show more warping in the bilayer than correlated domains. This can be attributed to the fact that, although lipid self-assembly allows lipids to interact attractively with each other for the most part, there is also repulsive interaction due to surface tension in domain borders as well as with the hydration water and the opposing bilayer on the surface of the domains. For example, the following figure (Figure 12) contains three distinctly different situations. Figure 12a displays a cross section of a DLPC- $L_0$  phase in DUPC- $L_d$ . Due to the fact that their aliphatic chains have similar lengths, so they can be stacked onto each other without attached difficulty. In this case, only lineal tension between domains is relevant. At the nanoscale, the lineal tension due to perimeter surface of the domain is still a major contributing factor to the overall tension.

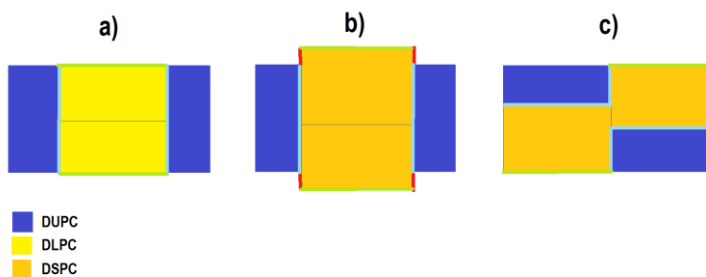


Figure 12: schemes of correlation and anticorrelation phenomena between leaflets in lipid bilayers. Red lines show unfavorable lipid-water lineal tension

With DLPC, the side chains in both saturated and unsaturated lipids are of similar length, and thus synchronization between  $L_o$  domains on both sides occurs. However, with the case of DSPC (Figure 12b), which has a longer chain, saturated lipids would protrude from the surface of the membrane on both sides, and thus increase the lineal tension of the domain perimeter because of contact with the surrounding aqueous environment, which is energetically very costly. This situation, which is not displayed when using DLPC, is therefore highly unstable.

For this reason, the leaflets may shift parallelly and desynchronized on either side, showing anticorrelation (Figure 12c), in order to decrease the linear tension between the  $L_o$  perimeter and the aqueous surroundings. While this also increases the interleaflet surface tension, this effect is only noticeable at bigger scale. This can be seen in the computational results, specifically in Figure 11f.

Therefore, the PC lipid used not only influences the organization of lipids within the leaflet, it also influences organization and structure between leaflets, which can have repercussion in membrane functionality [17-21]. On another note, at nanometric scale, the surface tension of a domain can be considered constant, but as the domain grows, surface tension experiences quadratic growth, and thus the domains might resynchronize at micrometric scale when it can compensate the linear tension with water.

To further analyze the results, GROMACS is also used to calculate the mean square displacement of each chemical species during the last 600 ns of simulation and the first frame as the reference. Only Brownian movement is considered, and movement restrained to the xy plane, where the bilayer is located. However, because I am working with periodic boundaries, if MSD were to be calculated indefinitely, a maximum would be reached. Therefore, if said maximum appears in the graph, the time frame is truncated to avoid it. The graphics obtained (Figure 13, Appendix 1) show that there is a lineal relation between time and MSD. This fits with the following model for liquid diffusion, where  $d$  stands for the dimensionality, and  $D$  the diffusion coefficient- Therefore, if regression for the data is done, and the slope is divided by four, the lateral diffusion coefficient is obtained (Table 2).

$$\langle \Delta r^2 \rangle = 2dDt$$

In general, the results fit with experimental [26-28] and computational [8] data consulted, which puts them at around  $10^{-7}$ - $10^{-8}$   $\text{cm}^2/\text{s}$ ; and thus, can be considered realistic. It is possible to confirm that there are two liquid phases, and that DUPC in general has bigger diffusion

coefficient than DLPC or DSPC, and thus higher mobility and fluidity. This correlates with the lipid raft model, because these are more rigid and “float” around the  $L_o$  phase.

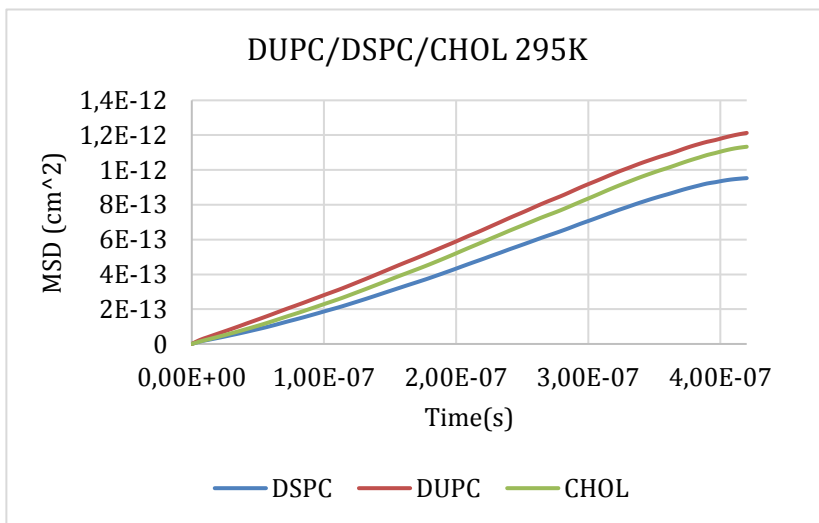


Figure 13: MSD graphic example, for DSPC-enriched bilayer at 295K during the last 600 ns of the CG MD simulation

D lateral (10 <sup>-7</sup> cm <sup>2</sup> /s)		
<b>Entry</b>	Lipid	295 K
1	DLPC	5,81
2	DUPC	6,66
3	CHOL	6,89
<b>Entry</b>	Lipid	295 K
5	DSPC	6,15
6	DUPC	7,59
7	CHOL	7,22

Table 2: Lateral diffusion coefficients from CG MD simulations at 295 K

## 7. CONCLUSIONS

Lipid vesicles with three different compositions (DOPC, DPPC/CHOL, and DOPC/DPPC/CHOL 0.342:0.340:0.320 molar, which mimic and simplify the structure of cell membranes, were successfully prepared via electroformation.

Vesicles were found to be generally spherical, and between 5 and 70  $\mu\text{m}$  in diameter, with 10-20  $\mu\text{m}$  being the most common bracket. DOPC vesicles were the smallest and most abundant, whereas DPPC/CHOL were the biggest but in less quantity. The latter is likely due to the increase of curvature and rigidity caused by cholesterol condensation and tighter packing.

Ternary vesicles lie between the two extreme cases. Using fluorescence microscopy, it is possible to distinguish between the micrometric  $L_0$  and  $L_d$  phases. Furthermore, some vesicles show pear-like shape due to the coexistence of two different surface tensions for each microdomain, and thus two different curvatures.

CG MD simulations using GROMACS for a DOPC/saturated lipid/CHOL 0.33:0.33:0.33 cubic 20x20x20 nm sized explicitly hydrated box with periodic boundaries were carried out at three different temperatures (285K, 290K, 295K). Two different kinds of saturated lipids were used: DLPC, which has a shorter aliphatic chain, and DSPC, which has a longer one.

In all simulations, liquid phase segregation was observed at the nanometric scale, with  $L_0$  and  $L_d$  phases forming, which are akin to the lipid rafts model found in *in-vivo* membranes. Quenched systems, or systems at lower temperatures, show less fluctuation and less irregular  $L_0$  domains than systems at higher temperature.

In systems containing DLPC, correlation between domains on either side of bilayer was observed, whereas in DSPC-containing systems, anticorrelation between domains was observed as well as bilayer warping and bending as a result of said anticorrelation. This anticorrelation is said to have a key role in regulating membrane functionality.

Secondly, the mean square displacement in the bilayer plane for the last 600 ns of each simulation is calculated and graphed for each chemical species. The relationship between time and mean square displacement is lineal, and within realistic magnitude, and thus it can be confirmed that liquid phases have been formed.

From this information the lateral diffusion coefficients can be obtained, and it was determined that unsaturated lipids of the  $L_0$  phase have higher diffusion than saturated lipids, analogous to the tighter packing in lipid rafts that makes them more rigid and less mobile.

To sum up, the final conclusion is that the PC type not only determines organization in the membrane on the same leaflet, but also between leaflets, in liquid phase segregated lipid bilayers.









## 8. REFERENCES AND NOTES

1. Karnovsky, M. J., Kleinfeld, A. M., Hoover, R. L., & Klausner, R. D. The concept of lipid domains in membranes. *J. Cell. Bio.* **1982**, *94*, 1-6.
2. Lingwood, D., & Simons, K. Lipid Rafts as a Membrane-Organizing Principle. *Science*. **2010**, *327*(5961), 46–50.
3. Simons, K., & Toomre, D. Lipid rafts and signal transduction. *Nat. Rev. Mol.* **2000**, *1*(1), 31–39.
4. Korade, Z., & Kenworthy, A. K. Lipid rafts, cholesterol, and the brain. *Neuropharmacology*. **2008**, *55*(8), 1265–1273.
5. Munro, S. Lipid Rafts: Elusive or Illusive? *Cell*. **2003**, *115*(4), 377–388
6. Owen, D. M., Magenau, A., Majumdar, A., & Gaus, K. Imaging Membrane Lipid Order in Whole, Living Vertebrate Organisms. *Biophys. J.* **2010**, *99*(1), L7–L9.
7. Nickels, J. D., Chatterjee, S., Stanley, C. B., Qian, S., Cheng, X., Myles, D. A. A., ... Katsaras, J. The in vivo structure of biological membranes and evidence for lipid domains. *PLoS Biology*. **2017**, *15*(5).
8. Risselada, H. J., & Marrink, S. J. The molecular face of lipid rafts in model membranes. *Proc. Natl. Acad. Sci. U.S.A.* **2008**, *105*(45), 17367 – 17372.9.
9. Schäfer, L. V., de Jong, D. H., Holt, A., Rzepiela, A. J., de Vries, A. H., Poolman, B., ... Marrink, S. J. Lipid packing drives the segregation of transmembrane helices into disordered lipid domains in model membranes. *Proc. Natl. Acad. Sci. U.S.A.* **2011**, *108*(4), 1343 – 1348.
10. Veatch, S. L., & Keller, S. L. Separation of liquid phases in giant vesicles of ternary mixtures of phospholipids and cholesterol. *Biophys. J.* **2003**, *85*(5), 3074–3083.
11. Almendro Vedia, V. G., Natale, P., Chen, S., Monroy, F., Rosilio, V., & López-Montero, I. iGUVs: Preparing Giant Unilamellar Vesicles with a Smartphone and Lipids Easily Extracted from Chicken Eggs. *J. Chem. Ed.* **2017**, *94*(5), 644–649.
12. Van Der Spoel, D., Lindahl, E., Hess, B., Groenhof, G., Mark, A. E., & Berendsen, H. J. C. GROMACS: Fast, flexible, and free. *J. Comput. Chem.* **2005**, *26*(16), 1701–1718.
13. Monticelli, L., Kandasamy, S. K., Periole, X., Larson, R. G., Tieleman, D. P., & Marrink, S.-J. (2008). The MARTINI Coarse-Grained Force Field: Extension to Proteins. *J. Chem. Theory Comput.* **2008**, *4*(5), 819–834.
14. Silvius, J. R. Role of cholesterol in lipid raft formation: lessons from lipid model systems. *Biochim. Biophys. Acta, Biomembr.* **2003**, *1610*(2), 174–183.
15. Crane, J. M., & Tamm, L. K. Role of Cholesterol in the Formation and Nature of Lipid Rafts in Planar and Spherical Model Membranes. *Biophys. J.* **2004**, *86*(5), 2965–2979.
16. Veatch, S. L., & Keller, S. L. Miscibility Phase Diagrams of Giant Vesicles Containing Sphingomyelin. *Phys. Rev. Lett.* **2005**, *94*(14), 148101.
17. Keller, S. L., Gruner, S. M., & Gawrisch, K. Small concentrations of alamethicin induce a cubic phase in bulk phosphatidylethanolamine mixtures. *Biochim. Biophys. Acta, Biomembr.* **1996**, *1278*(2), 241–246.
18. Brown, M. F. Modulation of rhodopsin function by properties of the membrane bilayer. *Chem Phys Lipids*. **1994**, *73*(1), 159–180.
19. Burack, W. R., & Biltonen, R. L. Lipid bilayer heterogeneities and modulation of phospholipase A2 activity. *Chem Phys Lipids*. **1994**, *73*(1), 209–222.

20. Suzuki, K. G. N., Fujiwara, T. K., Edidin, M., & Kusumi, A. Dynamic recruitment of phospholipase C $\alpha$  at transiently immobilized GPI-anchored receptor clusters induces IP $_3$ -Ca $^{2+}$  signaling: single-molecule tracking study 2. *J. Cell Biology*. **2007**, 177(4), 731 LP – 742.
21. Anderson, R. G. W., & Jacobson, K. A Role for Lipid Shells in Targeting Proteins to Caveolae, Rafts, and Other Lipid Domains. *Science*. **2002**, 296(5574), 1821 LP – 1825.
22. Marrink, S. J., Risselada, H. J., Yefimov, S., Tieleman, D. P., & de Vries, A. H The MARTINI Force Field: Coarse Grained Model for Biomolecular Simulations. *J Phys Chem B*. **2007**, 111(27), 7812–7824.
23. Marrink, S. J., de Vries, A. H., & Mark, A. E. Coarse Grained Model for Semiquantitative Lipid Simulations. *J Phys Chem B*. **2004**, 108(2), 750–760.
24. Marrink, S. J., de Vries, A. H., Harroun, T. A., Katsaras, J., & Wassall, S. R. (2008). Cholesterol Shows Preference for the Interior of Polyunsaturated Lipid Membranes. *J Am Chem Soc*. **2008**, 130(1), 10–11.
25. Wassenaar, T. A., Ingólfsson, H. I., Böckmann, R. A., Tieleman, D. P., & Marrink, S. J. Computational Lipidomics with insane: A Versatile Tool for Generating Custom Membranes for Molecular Simulations. *J Chem Theory Comput*. **2015**, 11(5), 2144–2155.
26. Lindblom, G., & Orädd, G. Lipid lateral diffusion and membrane heterogeneity. *Biochim. Biophys Acta, Biomembr*. **2009**, 1788(1), 234–244.
27. Filippov, A., Orädd, G., & Lindblom, G. The Effect of Cholesterol on the Lateral Diffusion of Phospholipids in Oriented Bilayers. *Biophys J*. **2003**, 84(5), 3079–3086.
28. Kahya, N., Scherfeld, D., Bacia, K., Poolman, B., & Schwille, P. Probing Lipid Mobility of Raft-exhibiting Model Membranes by Fluorescence Correlation Spectroscopy. *J. Biol. Chem*. **2003**, 278, 28109

## 9. ACRONYMS

CG: Coarse grained

Chol: cholesterol

DLPC: 1,2-dilauroyl-sn-glycero-3-phosphocholine

DOPC: 1,2-dioleoyl-sn-glycero-3-phosphocholine

DPPC: 1,2-dipalmitoyl-sn-glycero-3-phosphocholine

DSPC: 1,2-distearoyl-sn-glycero-3-phosphocholine

DUPC: 1,2-dilinoleyl-sn-glycero-3-phosphocholine

GROMACS: Groningen Machine for Chemical Simulations

ITO: indium tin oxide

LED: light emitting diode

Lo: liquid-ordered phase

Ld: liquid-disordered phase

MARTINI: CG force field for biomolecules and simplified biological systems

14:0 NBD-DMPE: 1,2-dimyristoyl-sn-glycero-3-phosphoethanolamine-N-(7-nitro-2-1,3-benzoxadiazol-4-yl) (ammonium salt)

MSD: mean square displacement

OM: optical microscopy

PC: phosphatidylcholines

VMD: Visual Molecular Dynamics



# APPENDICES





## APPENDIX 1: MEAN SQUARED DISPLACEMENT GRAPHICS

